Electron Backscattering Diffraction (EBSD), a complementary analytical approach for the microstructural characterisation of ancient materials by Electron Microscopy

J. Pérez-Arantegui (1)* and A. Larrea (2)

(1) Instituto Universitario de investigación en Ciencias Ambientales de Aragón (IUCA), Universidad de Zaragoza, Pedro Cerbuna 12, 50009 Zaragoza, Spain

(2) Instituto de Ciencia de Materiales de Aragón, CSIC-Universidad de Zaragoza, María de Luna 3, 50018 Zaragoza, Spain.

* Corresponding author: Josefina Pérez-Arantegui

e-mail: jparante@unizar.es

Phone number: +34 976 76 22 55

Fax number: +34 976 76 12 92

Abstract

Since the development of the Electron Backscattering Diffraction (EBSD) technique, Scanning Electron Microscopy (SEM) has become a powerful tool for characterising the local crystallography of bulk materials at nanoscale. Although EBSD is now a well-established characterisation method in materials science, it has been rarely used in the fields of art and archaeology, and nearly exclusively in metallic materials. However, the possibilities offered by EBSD could be also exploited to characterise ancient materials and to highlight their local crystallography, for instance in the study of natural or artificial pigments. This paper discusses the potential of EBSD as outlined in studies published to date and from its application with an ancient material - the Egyptian blue - in the identification of crystalline phases, in drawing phase maps, as well as in the extraction of several microstructural parameters, such as the grain size and the aspect ratio distribution of phases.

Keywords: EBSD, electron microscopy, materials, characterisation, art, archaeology, cuprorivaite

1. Scanning Electron Microscopy and Electron Backscattering Diffraction

Scanning electron microscopy (SEM) has been long used due to its unmatched ability, both on powdered and bulk samples, to combine high-resolution images with elemental chemical analysis by means of Energy Dispersive Spectroscopy (EDS). The spatial resolution of the images obtained in current field emission SEM is bellow 1 nm, whereas EDS systems can now detect elements heavier than boron (Z=5) and draw compositional maps with a spatial resolution below 1 μm. However, for decades there was no means to obtain crystallographic information in a SEM specimen in a fast and simple manner. Researchers interested in combining high-resolution images and elemental chemical analysis with crystallographic information were thus forced to use only Transmission Electron Microscopy (TEM). TEM is very powerful, but having to work with electron transparent specimens involves difficult sample preparation and limits the observation to small areas of the sample. However, since the development of Electron Backscattering Diffraction (EBSD) in the 1990s, SEM has become a powerful tool for characterizing the local crystallography in large areas of bulk materials with a spatial resolution as small as ~10-20 nm [1]. Although EBSD is now a well-established characterisation method in materials science, in the rare cases where it has been used in the fields of art and archaeology, these have been nearly exclusively in metallic materials [2].

EBSD is based on the acquisition of divergent-beam-electron diffraction patterns in a SEM, called Kikuchi patterns after their first description by Seishi Kikuchi [3], in back reflection geometry. Although the acquisition of EBSD patterns was already reported in the 1950s [4] and scanning electron microscopes became commercially available in the 1960s, the use of EBSD in materials science was very limited until the development of high-sensitivity recording cameras and fast automated computerized methods for on-line pattern analysis.

Methods for the fully automated indexation of EBSD patterns were developed in the 1990s [5] through the Hough transformation of the patterns [6]. Commercial EBSD systems soon became available and the so-called Orientation Imaging Microscopy™ (OIM) rapidly spreads throughout materials characterisation laboratories. Commercial EBSD systems are now a common and moderate-price SEM accessory. Currently they can be used to record, store and index individual EBSD patterns in about 10 ms and to plot large area maps of bulk samples representing the crystallographic orientation of each pixel, as well as another microstructural parameters. The development of modern EBSD is the result of the collective efforts of many scientists, and readers interested in this matter can consult the excellent review written by one of these scientists - D.J. Dingley [7].

In an EBSD experiment, the vertical electron beam hits the sample's surface at an angle of about 70º (the sample is tilted towards the EBSD detector), producing diffracted electrons. These diffracted electrons form a pair of Kossel cones (*hkl* and $\overline{h}\overline{k}\overline{l}$) for each reflecting plane. The projection of the Kossel cones on the EBSD detector screen produces pairs of Kikuchi lines, also known as Kikuchi bands including the region between them (Fig. 1). Although the mechanisms related to the formation of band contrasts are quite complex, it is easier to understand that, as the Kossel cones are centred at a point on the diffracting planes, they reflect the crystal symmetry of the electron interaction point, thus enabling the spatially resolved crystallographic identification in the SEM. The position of the Kikuchi bands in the detector screen also reveals the crystallographic orientation of the analyzed grains.

EBSD experiments are performed on flat faces of cleaved crystals or, more commonly, on polished specimens. EBSD analysis of non-flat samples is also possible, however shadowing of the backscattered electrons in the sample itself prevents orientation maps from being

obtained and limits these experiments to the acquisition of diffraction patterns of protruding grains for phase identification. The polished EBSD specimens are generally prepared using conventional metallographic methods. The only special care needed is to ensure that the sample surface is free of damage, because the EBSD patterns are generated from the ~40 nm top surface layer [8]. The strains introduced by overly aggressive sample polishing would blur the Kikuchi bands. Thus the specimen is prepared using a progressive lapping and polishing method to eliminate any strain created in the previous step. For a common ceramic sample, two grinding and two polishing steps using a low load and rotation speed of the polishing wheel, followed by a final polishing using colloidal silica, are generally sufficient. The same methods that produce well-prepared specimens for high contrast SEM backscattering observations using low-energy incident electrons, which are the most sensitive to the quality of the specimen surface, are often good choices for EBSD sample preparation. However, differential polishing needs to be kept to a minimum to prevent shadows in the grain boundaries due to the tilted position of the sample. This effect limits the minimum grain size in the orientation maps. Special care should be taken to adjust the duration of the final step using colloidal silica, and long polishing times result in good quality patterns, however can lead to differential polishing between the phases. Colloidal silica should also be avoided if there are components that are sensitive to the alkaline pH of the solution in the sample, in order to avoid chemical reactions that may modify the composition. In this case other polishing compounds, such as acidic alumina suspensions, could be used. In our experience EBSD specimen preparation of a common sample is not much more difficult than for daily SEM, and certainly less difficult than for TEM. However, it is true that EBSD specimen preparation of delicate samples, mixing small grains of hard and soft phases, is always very challenging. Compared to TEM specimen preparation, the quality of the surface finish is

similar, though luckily only one side needs polishing and, even better, a thin film does not need to be prepared.

Spatial resolution of the EBSD technique is limited to 10-20 nm by the effect of the electron dispersion in the bulk sample [9], while the spatial resolution in modern TEMs using Convergent Beam Electron Diffraction (CBED) is only limited by the need for a minimum number of atoms to behave like a crystal, the practical limit being about 1 nm. In fact, electron diffraction has been conventionally used in TEM for decades. Unlike TEM, with EBSD large areas of bulk samples can be studied with fast and automated acquisition and analysis of the patterns. Both techniques have developed counter-attack strategies to overcome their own limitations. On the one hand, in TEM it is now possible to plot orientation maps in an automated way using the Precession Electron Diffraction (PED) technique [10], where the focused beam is scanned at a constant angle around the optic axis [11]. Using a slower procedure than EBSD, they achieve a spatial resolution of up to 1 nm. On the other hand, it is now possible to perform EBSD experiments in the SEM in transmission mode (t-EBSD, also referred to as TKD [12]) to improve the spatial resolution below 10 nm. Generally speaking, SEM-EBSD is better for fast and large automated electron diffraction maps of bulk samples, whereas TEM-PED is more appropriate for high-resolution orientation maps of small, roughly tens of square micrometers, thin-film samples.

Now that EBSD has been established as a common tool for material characterization, two main development lines are underway: quantitative strain mapping and accurate phase identification. EBSD strain mapping has always been possible in EBSD due to the presence of dislocations in the diffraction volume that produce pattern blurring. Thus, we can use the pattern sharpness (through the so-called *Band-Contrast* component) to represent, in a

qualitative manner, the specimen strain. Strain mapping can also be performed more sophistically by calculating the scalar misorientation between the pixels of an individual grain [13]. High-sensitivity cross-correlation analysis between the strained EBSD patterns and a strain-free reference pattern is currently used to obtain quantitative strain information with a sensitivity of about 10^{-4} [14]. One of the problems of applying this method to polycrystalline materials is the need for accurate pattern simulation, because it is not generally possible to have experimental strain-free patterns in random orientations. To overcome this drawback, many-beam dynamical calculations have been applied [15] and have also led to important developments in accurate phase identification that are already commercially available [16].

To sum up, in an EBSD experiment a set of backscattering diffraction patterns are collected from the well-polished surface of a bulk sample, one pattern by each pixel of the surface image. The acquisition time is usually from 10 to 200 ms per pixel and the best available spatial resolution is 10-20 nm. These patterns are indexed on-line, i.e. the crystalline phase to which the grain belongs is identified and its 3D crystallographic orientation determined, but usually they are subsequently re-analysed off-line using more sophisticated routines. From this information it is possible to plot maps using different components to provide information on diverse microstructural and crystallographic parameters: phase identification, crystallographic orientation (including grain size and morphological grain statistics), strains, lattice correlation boundaries, and sigma values obtained in the Coincidence Site Lattice (CSL) [17] framework to classify boundaries, etc. The possibilities offered by the EBSD experiments are increasingly used for material characterisation and can also be exploited to characterise ancient materials and highlight their local crystallography.

2. EBSD in the fields of Art and Archaeology

2.1. Metallic materials

In art and archaeology, EBDS has been more often used to study metallic samples, mainly focusing on the metallurgical properties of iron, silver or copper alloys. The earliest references in the literature correspond to the research by Mapelli, Nicodemi and co-workers on ancient swords and nails aimed at improving knowledge of the metallurgical techniques related to iron materials [18-21]. EBSD enabled the orientation map of each scanning area to be defined and to determine the Orientation Distribution Function (ODF). SEM-EBSD analysis identified the crystallographic textures (the preferential orientation of the crystals) and their distribution within different areas of the samples. This then highlighted a forming process that produced interesting mechanical properties in the metal products.

Sullivan and co-workers also focused on the characterisation of iron alloys, used in ancient Indian swords [22-25]. EBSD was used to analyse the nature of the carbides in ancient wootz steel blades because these carbides are useful in determining the deformation and metallurgical history. Wootz is the name given to a crucible steel manufactured in India. Ancient wootz objects are classed as high carbon (hypereutectoid) crucible steels and are characterized by high strength, hardness, and resistance to wear, and especially their attractive surface pattern [24]. From EBSD data, crystallographic orientation, spatial distribution, and/or ripening were displayed in high-magnification Euler angle maps of the fine carbide phase. As well as obtaining the crystallographic orientation from the Kikuchi patterns, the contrast of the patterns was also mapped through the *Band Contrast* component. This provides a measure of the degree of lattice disruption and thus reveals low-angle grain boundaries and dislocation density. *Band Contrast* maps in a grey-scale represent to some extent the presence of strains and can highlight important microstructural information.

Azoulay and co-workers proposed EBSD as a suitable method to study ferrous corrosion products on iron archaeological objects [26]. An understanding of corrosion mechanisms requires a thorough investigation of the chemical, mechanical and morphological characteristics of the Fe(II)-based layer that develops between the metal surface and the environment. SEM-EBSD offers the possibility of phase characterisation and microstructural study under vacuum and consequently protected from air. In Azoulay and co-workers' study, firstly EBSD patterns were used to identify crystalline phases and the results were compared to those obtained by micro-Raman spectroscopy. Local EBSD maps were then obtained in two scanning modes to reveal the repartition of mineral phases in a heterogeneous section and to obtain the relative crystallographic orientations of grains. Finally, various phases, such as magnetite, siderite and ferrous hydroxychloride, β-$Fe_2(OH)_3Cl$, were fully characterised by EDS/EBSD-SEM, however electron diffraction patterns were not obtained from some of the compounds present in the studied samples. This could have been due to poorly ordered and poorly crystallised phases, highly heat-sensitive compounds, or to problems during sample preparation.

Silver alloys are another type of metallic material that have also been characterised by EBSD. Wanhill used automated EBSD to improve the analysis and assessment of corrosion-induced embrittlement in ancient silver [27]. Corrosion, and also microstructurally-induced embrittlement, can have catastrophic consequences for the object's integrity, which is why recognising these mechanisms and understanding the extent of the problem are essential for conserving ancient silver artefacts. Lejček and co-workers studied the structure/property relationship in polycrystalline materials from the selective intergranular corrosion observed in archaeological artefacts manufactured from a Ag-1%Cu alloy (dated to the 10th century

AD) [28]. EBSD enabled individual grain boundaries to be identified and their crystallographic maps were then evaluated to examine the selective corrosion attack: the general grain boundaries were preferably attacked.

Northover and Northover used EBSD to compare the microstructure of modern and ancient (about 2500 years old) cast silver-copper alloys [29]. The work used a combination of SEM, EDS, EBSD, TEM, Scanning Transmission Electron Microscopy (STEM) and Optical Microscopy to explore the microstructure. EBSD *Band Contrast* and *Crystallographic Orientation* maps were plotted to study different areas. Both alloys were characterised by Ag-rich dendrites with a few pools of eutectic and occasional cuprite particles with an oxidised rim on the outer surface. EBSD showed that the dendrites had a complex internal structure, often involving extensive twinning. The ancient cast Ag-Cu alloys also showed twinning in a similar as-cast grain structure, however EBSD orientation images suggested cellular growth at the boundaries, which was not observed in any of the modern Ag-Cu alloys. Although TEM diffraction patterns were useful in determining the crystallography of various fine Cu-rich precipitates, EBSD is the only technique that can provide the necessary crystallographic information over a wide enough area, in order to locate and examine a sufficient length of as-cast grain boundaries thus identifying and characterising any modifications. Wanhill and co-workers had already used EBSD to illustrate boundary changes identified as age-related in Ag-alloys from several archaeological contexts [30].

Peruzzo and co-workers also exploited EBSD for the characterisation of bronzes, Cu-Sn artefacts [31,32]. EBSD was used to measure crystal orientation and phase distribution, and to interpret the elasticity of some objects based on their microstructure.

2.2. Ceramics and vitreous materials

Compared to metals, the study of ceramics involves a variety of problems for EBSD investigations such as: (i) a complicated crystal structure, (ii) difficult surface preparation, and (iii) problems arising from the low conductivity of the ceramic materials [33]. This probably explains the lack of EBSD applications in ancient ceramics.

One example of EBSD in ceramic studies is for the characterisation of a porous, hard-paste porcelain-like material (Cyfflé's *Terre de Lorraine* wares) [34]. The authors used a multiple approach by X-Ray Fluorescence (XRF), X-Ray Diffraction (XRD), SEM, EDS and EBSD to determine the porosity, bulk, major, minor and trace element compositions, as well as the composition and the proportion of their constituent phases. EBSD was used to identify some of the phases (α-quartz and mullite) contained in the aluminous-siliceous ceramic bodies, some of which are amorphous. The aim was to understand the nature of the raw materials and the possible firing temperatures used in the manufacture.

Another example of EBSD used to study pottery pigments was reported by Peruzzo and co-workers [35]. Tiny particles under the glaze were responsible for the black decoration in 9th-10th century AD ceramics from Turkmenistan. The chemical composition of these particles was consistent with that of a manganese oxide (or hydroxide), however the nature of the pigment was not clear. EBSD analysis, in fact, proved the non-crystallinity of all the analysed particles, according to the absence of diffraction patterns. It was thus possible to demonstrate that the black pigment was not a crystalline phase and did not correspond to any of the previously proposed manganese-containing phases.

Other possible uses of EBSD include analyses of vitreous materials, such as ceramic glazes or glass. These types of amorphous materials can contain crystalline micro-particles related to the production technology (e.g. raw materials, firing process) or to the optical properties (e.g. opacity and colour). EBSD analysis can help to define the nature of these crystalline particles, which are impossible to distinguish by conventional methods in bulk samples such as XRD or EDS-SEM. This limitation can be due to one or more of the following reasons: (i) the particles are too small; (ii) there are too few particles; (iii) the particles are too strictly integrated in a complex texture to provide a recognizable signal, or to be separated and concentrated; and (iv) their chemical composition does not enable different minerals to be distinguished [35]. For instance, the yellow-orange decoration of Italian Sgraffito polychrome slipware (second half of the 15th to the 16th century AD) contained micrometric crystals of synthetic bindheimite, a lead antimonate, dispersed in the lead-based glaze and responsible for the colour [35]. The same authors also used EBSD to identify near-millimetric residues of raw materials, such as metallic copper, cuprite and the micrometric iron-containing heterogeneities, in red mosaic glasses by means of the backscattered electron diffraction patterns.

One of the main difficulties in the EBSD study of glassy materials may be due to the polishing of the specimen in the preparation of the sample. In fact, a good surface state is needed to produce a sufficiently sharp pattern to be indexed, and differences in strength between the tiny crystal particles and the surrounding matrix could cause a differential polishing of the crystal surface. As indicated in Section 1, since the specimen is ~70º tilted with respect to the electron beam, there is shadowing in the boundary between the glass and the crystalline phases, which prevents any analysis of the small particles. It has been demonstrated that a compact and amorphous vitreous matrix is appropriate for an EBSD

characterisation of the crystalline phases. However, the hardness of the crystalline particles should be comparable to that of the glassy matrix.

2.3. Minerals, pigments and paintings

In the past few years EBSD has also become one of the common methods to quantify complete microfabrics of different rock types. However, only one application of the EBSD method for the study of marble microstructures has been published [36]. The authors of that study used EBSD, together with TEM, SEM, reflected light imaging and cathodoluminescence, to define the origin of ancient marble within, and between, different regions. In the case of marbles with second-phase unaffected microstructures with mean grain sizes at the micrometre scale, EBSD was specifically applied for the automatic determination of the microfabric of calcite, i.e. its grain size and crystallographic orientation. Second-phase corrected microstructures were used to define geological areas of similar grain sizes, which corresponded to specific metamorphic or isothermal regions.

Gambirasi *et al.* [2] discussed the feasibility of EBSD analysis to study heterogeneous matrices in very small samples of paint layers collected from paintings, an important field dealing with the conservation of cultural heritage. These materials also require the clear identification of inorganic and crystalline components, such as pigments and their alteration products. Painting samples, usually resin-mounted in cross-sections, cannot be easily studied by XRD because of the difficulty in selectively investigating each individual pigment grain in the different paint layers (the pigment particles often are very small and/or very few, and embedded in an organic binding media). TEM is also hard to apply because specimen preparation in this case is extremely difficult. The authors applied EBSD on two reference pigments (azurite and cinnabar) and on two real painting samples from Italy dated to 1514,

all prepared as cross-sections. EBSD patterns highlighted the presence of azurite in one of the real samples and cinnabar in the second painting sample. The investigations on both samples demonstrated that polishing real samples is particularly challenging, since the heterogeneous paint layers can be composed of materials with different degrees of hardness as well as distinct behaviours during the polishing process. It has also been observed that harder pigments, such as azurite, produced better patterns than the softer ones, such as cinnabar.

3. The characterisation of Egyptian blue: an example of EBSD in ancient pigments

Although the results reported in Section 2 were obtained from a limited number of cases, EBSD appears to be promising in identifying pigments employed in works of art and in highlighting their local crystallography. Its suitability can be illustrated by highlighting how it was exploited to study a particular artificial pigment, Egyptian blue. The material considered in this study belongs to a collection of more than 250 balls (1-2 cm diameter) of pigment (see inset in Fig. 2) found in the Roman archaeological site of La Cabañeta (Zaragoza, Spain), probably the ancient *Castra Aelia*, founded in the 2nd century BC in the middle Ebro valley, and destroyed in the 1st century BC [37]. A small fragment, about 3-4 mm long, of a broken ball was used for the study.

Egyptian blue has always interested specialists in terms of understanding its composition and manufacture, such as de Fontenay in 1874 [38] or Jope and Huse in 1940 [39]. Egyptian blue is a multicomponent material whose blue colour is due to the presence of calcium-copper tetrasilicate crystals (cuprorivaite, $CaCuSi_4O_{10}$). In ancient times it was generally produced by firing a mixture of quartz, lime, a copper compound and an alkali flux, producing a glassy mass or frit, and predominantly used as pigment [40]. Depending on the raw materials used and the production process followed, Egyptian blue shows a different bulk composition and

microstructure [40-43]. An in-depth study of the chemical and crystallographic composition can therefore highlight the features related to the origin and technology of the pigment found in archaeological contexts.

Many studies on Egyptian blue have been carried out using EDS-SEM, and complemented with XRD [41,42]. XRD provides a bulk analysis of the overall powdered material, however, a minimum amount of Egyptian blue is needed to produce a representative X-ray powder diffraction pattern. This minimum amount is typically larger than what is usually available for this type of pigment in archaeological remains. Hence the possibility of using a single sample preparation to obtain chemical, microstructural and crystallographic information by SEM-EDS and EBSD could be very useful for art and archaeometric studies. In the last few years Egyptian blue has also attracted the interest of material scientists, since the mineral cuprorivaite exhibits exceptionally high emission quantum efficiency in the near-infrared region [44,45].

Microstructural observations were performed using a Field Emission Scanning Electron Microscope (FESEM) model Merlin from Carl Zeiss NTS (Oberkochen, Germany). This microscope was equipped with an INCA350 Energy Dispersive Spectroscopy (EDS) apparatus from Oxford Instruments (Abingdon, Oxfordshire, United Kingdom). EBSD experiments were also performed with the same microscope using an HKL detection system from Oxford Instruments.

For the EBSD experiments, test specimens were prepared from the (porous) Egyptian blue samples by epoxy resin impregnation into conventional metallographic moulds. Surface preparation was accomplished using a progressive lapped and polishing method previously

tested on ceramic samples [46]. Thus, the specimens were first ground with SiC paper (P2500 and P4000) using a polishing wheel at 40 rpm and a load of 2.5 N. They were then polished with diamond slurry (3 μm and 1 μm of particle size, 120 rpm, 2.5 N load, 3 minutes each step) and with colloidal silica (OP-U Suspension from Struers, Denmark) at 100 rpm for 15 minutes. Finally, the specimens were carbon coated to avoid charging. Although in the SEM it is possible to use *in-situ* charge compensation for non-conductive samples [47], a sample coating was applied because the experiment was not limited by the grain size and high-energy incident electrons could be used.

In the microscope, the sample was tilted 70º, with respect to the incident beam, towards the CCD camera (1024 x 768 pixel) of the EBSD detector and placed at 14.5 mm of working distance (from the SEM pole piece). The accelerating voltage used was 30 kV and the probe current 1.2 nA. For each pixel of the scanned zones, the EBSD patterns (Kikuchi patterns) were recorded four times during 40 ms and averaged out to reduce noise. The total acquisition time was between 55 minutes and 5 hours, depending on the map size. After a first on-line fast indexation of the recorded EBSD patterns, the full set of patterns were analysed once again off-line following the more accurate Advanced Fit (AFI) routine of the Channel5 software (seven Kikuchi bands detected; Hough space resolution: 60) [48]. Where the angular deviation between the experimental and fitted pattern was higher than 2º, it was discarded and marked as non-indexed in the map.

In the previous SEM observations, the pigment showed a heterogeneous very porous microstructure (Fig. 2), with chemically different phases. The compositions (in wt%) of the three major phases were determined by EDS from the intensity of the characteristic cation peaks (oxygen content was determined by stoichiometry): i) a calcium-copper silicate

(66.3±0.4 SiO_2, 14.2±0.1 CaO and 19.5±0.4 CuO), ii) a high-sodium high-copper high-silica phase (68.7±0.7 SiO_2, 10.4±0.6 Na_2O and 11.2±1.0 CuO, together with 2.86±0.29 CaO, 0.86±0.11 MgO, 0.86±0.07 K_2O, 1.76±0.50 Al_2O_3, 1.84±0.40 FeO, 1.03±0.10 Cl), and iii) silica (SiO_2). The first phase matched with the cuprorivaite composition. The second phase was assumed to be an amorphous glassy phase, already mentioned by other authors who had studied Egyptian blue pigments from several origins [40,41,43]. This phase helped to connect the calcium-copper silicate crystals and other grains included in the porous microstructure.

In the EBSD experiments, several specimen zones were explored to check and quantify the presence of the cuprorivaite, the main phase associated with the Egyptian blue pigment. Three other Si-based crystallographic phases (wollastonite, quartz and tridymite) were considered to fit the experimental EBSD patterns. Their crystallographic parameters are listed in Table I. A typical pattern of a cuprorivaite grain showing the fitted bands is shown in Fig 3. Although the patterns were not of high quality, they were sufficient for automatic phase discrimination. Once every pixel of the scanned zone had been indexed, it was possible to build-up a phase map where a different colour was assigned to each phase. The noise in the orientation map was reduced by removing the isolated non-indexed points, which were filled using copies of the neighbouring points (if at least six were identical). This noise reduction process was iterated until convergence. The backscattered electron image, the electron forescatter image and the phase map of a 210x154 μm^2 zone scanned with 2 µm step size are shown in Fig. 4. The main phases are marked in Fig. 4a. In this phase map, the *Band Contrast* and *Band Slope* components were added to reveal various microstructural features. The blue areas in Fig. 4c correspond to cuprorivaite, the major phase in this case. In addition, various amounts of tridymite (green), quartz (yellow) and wollastonite (red) were observed. The non-indexed areas can be categorised into three regions. The bright areas in Fig. 4c correspond to

rough zones where shadowing in the backscattered beam produced artificial high contrast patterns. These rough zones stem from incomplete resin infiltration or grain breakage during specimen polishing. They were discarded in the map analysis by thresholding the image using the *Band Slope* component. The other dark non-coloured areas in Fig. 4c are non-diffracting glassy grains and resin-infiltrated pores. The pores were separated from the glassy zones by analysis of images obtained with backscattered electrons. Another larger area, with the same map representation as in Fig. 4c, is shown in Fig. 5.

From the phase maps it was also possible to obtain several microstructural parameters describing the samples. The percentage volume of the different phases in several analysed zones is presented in Table II, including the glassy phase. These quantitative phase data (not easy to calculate with other methodologies) could also highlight interesting differences between pigments. The grain size and aspect ratio distribution of cuprorivaite are shown in Fig. 6. Most of the grains had a size between 10 to 20 μm and present an aspect ratio close to 1. On the other hand, the main pole figures of tetragonal cuprorivaite are shown in Fig. 7. From the pole figures, it is evident that, as expected, there was no crystallographic texture in the samples. These microstructural characteristics of the cuprorivaite grains could be useful to identify the source of pigments from different archaeological findings.

4. Conclusions

The results discussed in the previous sections show that EBSD is suitable for identifying compounds used or generated in works of art or archaeological objects and for highlighting their local crystallography. Although good sample preparation is crucial to obtain well-resolved EBSD maps and phases, this step is no more difficult than other SEM preparations. EBSD also has good spatial resolution (10-20 nm) and shorter total times for obtaining and

processing the data, compared with other techniques, such as TEM. In addition, EBSD is the only technique that provides the necessary crystallographic information over a wide enough area. EBSD provides phase identification and crystallographic parameters that can be added to the chemical information of the ancient material, which would be very useful in archaeometric or conservation studies. Finally, using a single sample preparation to obtain chemical, microstructural and crystallographic information by SEM-EDS and EBSD would be very convenient in art and archaeometric studies.

Acknowledgments

The authors acknowledge funding by CTQ2011-24882 (Ministerio de Ciencia e Innovación) and MAT2012-30763 (Ministerio de Economía y Competitividad) projects, which are financed by the Spanish Government and the Feder program of the European Union. Part of the research was performed at the Servicio General de Apoyo a la Investigación-SAI, Universidad de Zaragoza (FESEM-EDS and EBSD).

References

[1] K. Z. Baba-Kishi, Review - Electron backscatter Kikuchi diffraction in the scanning electron microscope for crystallographic analysis, Journal of Materials Science 37 (2002) 1715-1746.

[2] A. Gambirasi, L. Peruzzo, S. Bianchin, M. Favaro, Electron Backscatter Diffraction in Conservation Science: Phase identification of pigments in paint layers, Microscopy and Microanalysis 19 (2013) 921-928.

[3] S. Kikuchi, Proc. Imp. Acad. Japan, 4 (1928) 271, 275, 354.

[4] M.N. Alam, M. Blackmann, D.W. Pashley, High angle Kikuchi patterns, Proc. Royal Society of London A221 (1954) 224.

[5] N.C.K. Lassen, D.J. Jensen, K. Conradsen, Image-processing procedures for analysis of electron back scattering patterns. Scanning Microscopy, 6 (1992) 115-121.

[6] P.V.C. Hough, Method and means for recognizing complex patterns, US Patent US3069654 A (1962).

[7] D.J. Dingley, The development of automated diffraction in scanning and transmission electron microscopy, in: A.J. Schwartz, M. Kumar, B.L. Adams (Eds.), Electron Backscatter Diffraction in Material Science, Kluwer Academic/Plenum Publishers, New York, 2000.

[8] A.J. Wilkinson, T.B. Britton, Strains, planes, and EBSD in materials science, Materials Today 15 (2012) 366-376.

[9] F.J. Humphreys, Characterization of fine-scale microstructures by backscatter electron diffraction (EBSD), Scripta Materialia 51 (2004) 771-776.

[10] E.F. Rauch, J. Portillo, S. Nicolopoulos, D. Bultreys, S. Rouvimov, P. Moeck, Automated nanocrystal orientation and phase mapping in the transmission electron microscope on the basis of precession electron diffraction, Zeitschrift Fur Kristallographie 225 (2010) 103-109.

[11] R. Vincent, P.A. Midgley, Double conical beam-rocking system for measurement of integrated electron-diffraction intensities, Ultramicroscopy 53 (1994) 271-282.

[12] P.W. Trimby, Orientation mapping of nanostructured materials using transmission Kikuchi diffraction in the scanning electron microscope, Ultramicroscopy 120 (2012) 16-24.

[13] L.N. Brewer, M.A. Othon, L.M. Young, T.M. Angeliu, Misorientation mapping for visualization of plastic deformation via electron back-scattered diffraction, Microscopy and Microanalysis 12 (2006) 85-91.

[14] A.J. Wilkinson, T.B. Britton, J. Jiang, P.S. Karamched, A review of advances and challenges in EBSD strain mapping, Iop, Emas 2013 Workshop: 13th European Workshop on Modern Developments and Applications in Microbeam Analysis, 55 (2014).

[15] A. Winkelmann, C. Trager-Cowan, F. Sweeney, A.P. Day, P. Parbrook, Many-beam dynamical simulation of electron backscatter diffraction patterns, Ultramicroscopy 107 (2007) 414-421.

[16] ESPRIT DynamicS, High Resolution EBSD Pattern Simulation. www.bruker.com/quantax.

[17] M.L. Kronberg, F.H. Wilson, Secondary recrystallization in copper, Transactions of the American Institute of Mining and metallurgical Engineers 185 (1949) 185-501.

[18] W. Nicodemi, C. Mapelli, R. Venturini, R. Riva, Metallurgical investigations on two sword blades of 7th and 3rd century BC found in Central Italy, ISIJ Int. 45 (2005) 1358-1367.

[19] C. Mapelli, W. Nicodemi, R. Venturini, R. Riva, Risultati derivanti da nuovi esami realizzati su manufatti bellici del VII a.C. e III a.C. rinvenuti in Etruria, Metallurgia Italiana 98 (2006) 15-24.

[20] C. Mapelli, W. Nicodemi, R.F. Riva, Microstructural investigation on a medieval sword produced in the 12th century AD, ISIJ Int. 47 (2007) 1050-1057.

[21] C. Mapelli, W. Nicodemi, R.F. Riva, M. Vedani, E. Gariboldi, Nails of the Roman Legionary at Inchtuthil, Metallurgia Italiana 101 (2009) 51-58.

[22] A. Sullivan, M. Barnett, R. Balasubramaniam, Preliminary EBSD analysis of wootz steel, Microscopy and Microanalysis 13, S02 (2007) 1104-1105.

[23] M.R. Barnett, A. Sullivan, R. Balasubramaniam, Electron backscatter diffraction analysis of ancient wootz steel blade from Central India, Mater. Charact. 60 (2009) 252-260.

[24] A. Sullivan, M. Barnett, EBSD Study of Indian Wootz Steel Artifacts to Infer Thermomechanical History by Observation of Carbide Distribution and Orientation, Micros. Today 18 (2010) 16-25.

[25] V. Kumar, R. Balasubramaniam, P. Kumar, Microstructure evolution in deformed ultrahigh carbon low alloy (Wootz) steel, Mater. Sci. Forum 702-703 (2012) 802-805.

[26] I. Azoulay, E. Conforto, P. Refait, C. Rémazeilles, Study of ferrous corrosion products on iron archaeological objects by electron backscattered diffraction (EBSD), Applied Physics A 110 (2013) 379-388.

[27] R.J.H. Wanhill, Embrittlement of ancient silver, J. Failure Anal. Prevent. 5 (2005) 41-54.

[28] P. Lejček, A. Jäger, V. Gärtnerová, J. Vaníčková, J. Děd, J. Haloda, Structure/property relationship in intergranular corrosion of archaeological silver artefacts, Mater. Sci. Forum 638-642 (2010) 2852-2857.

[29] S.M. Northover, J.P. Northover, Microstructures of ancient and modern cast silver-copper alloys, Materials Characterization 90 (2014) 173-184.

[30] R.J.H. Wanhill, T. Hattenberg, J.P. Northover, EBSD of corrosion, deformation and precipitation in the Gundestrup cauldron, in: A.C. Ferreiro da Silva, P. Menino Homem (Eds.), Ligas Metálicas: Investigação e Conservação, Faculdade de Letras da Universidade do Porto, Porto, 2008, pp. 47-61.

[31] F. Zaghis, L. Peruzzo, G. Salviulo, G. Molin, A new approach in studying ancient Cu–Sn artifacts: measure of crystal orientation and phase distribution by EBSD analysis, XX IUCr, Florence, Italy, 23–31 August 2005, Acta Crystallographica A61, Supplement (2005) C493.

[32] L. Peruzzo, D. Ferro, V. Virgili, I. Calliari, S. Buson, The contribution of SEM-EBSD analysis to a microstructural interpretation of the elasticity of ancient fibulae springs, in: N. Meeks, C. Cartwright, A. Meek, A. Mongiatti (Eds.), Historical Technology, Materials and Conservation: SEM and Microanalysis, Archetype Publications, London, 2012, pp. 185-187.

[33] M.R. Koblischka, A. Koblischka-Veneva, Applications of the electron backscatter diffraction technique to ceramic materials, Phase Transitions 86 (2013) 651-660.

[34] M. Maggetti, J. Rosen, C. Neururer, V. Serneels, Paul-Louis Cyfflé's (1724-1806) *Terre de Lorraine*: A technological study, Archaeometry 52 (2010) 707-732.

[35] L. Peruzzo, F. Fenzi, P.A. Vigato, Electron Backscatter Diffraction (EBSD): A new technique for the identification of pigments and raw materials in historic glasses and ceramics, Archaeometry 53 (2011) 178-193.

[36] A. Ebert, E. Gnos, K. Ramseyer, C. Spandler, D. Fleitmann, D. Bitzios, D. Decrouez, Provenance of marbles from Naxos based on microstructural and geochemical characterization, Archaeometry 52 (2010) 209-228.

[37] J. Pérez-Arantegui, A. Gil, L. Ventolá, M. Vendrell, J.A. Mínguez, Importations of highly prized products to inland eastern Iberia during the Roman republican period (2nd and 1st centuries BC): the case of Egyptian Blue pigment through its archaeometric study, 40th International Symposium on Archaeometry, Los Angeles, USA, Abstract Book (2014) 119.

[38] H. de Fontenay, Note sur le bleu égyptien, Annales de chimie et physique [5] 2 (1874) 193-199.

[39] E.M. Jope, G. Huse, Examination of 'Egyptian Blue' by X-ray powder photography, Nature 146 (3688) (1940) 26.

[40] G.D. Hatton, Production of Egyptian Blue and Green Frits, in: M.S. Tite, A.J. Shortland, (Eds.), Production Technology of Faience and Related Early Vitreous Materials, Monograph 72, University School of Archaeology, Oxford, 2008, pp. 147-185.

[41] S. Pagès-Camagna, S. Colinart, C. Coupry, Fabrication processes of archaeological Egyptian blue and green pigments enlightened by Raman microscopy and scanning electron microscopy, J. Raman Spectroscopy 30 (1999) 313-317.

[42] P. Bianchetti, F. Talarico, M.G. Vigliano, M.F. Ali, Production and characterization of Egyptian blue and Egyptian green frit, J. Cultural Heritage 1 (2000) 179-188.

[43] G.D. Hatton, A.J. Shortland, M.S. Tite, The production technology of Egyptian blue and green frits from second millennium BC Egypt and Mesopotamia, J. Archaeological Science 35 (2008) 1591-1604.

[44] G. Accorsi, G. Verri, M. Bolognesi, N. Armaroli, C. Clementi, C. Miliani, A. Romani, The exceptional near-infrared luminescence of cuprorivaite (Egyptian blue), Chemical Communications (23) (2009) 3392-3394.

[45] D. Johnson-Mcdaniel, C.A. Barrett, A. Sharafi, T.T. Salguero, Nanoscience of an ancient pigment, J. American Chemical Society 135 (2013) 1677-1679.

[46] S. Serrano-Zabaleta, M.A. Laguna-Bercero, L. Ortega-San-Martín, A. Larrea, Orientation relationships and interfaces in directionally solidified eutectics for solid oxide fuel cell anodes, J. European Ceramic Society 34 (2014) 2123-2132.

[47] S. Serrano-Zabaleta, A. Larrea, H. Stegmann, C. Waltenberg, Electron backscatter diffraction analysis of non-conductive samples using in-situ charge compensation, Microscopy and Analysis (8) (2013) 23-27.

[48] Channel 5. Oxford Instruments HKL®. HKL Technology 2006. Denmark.

[49] A. Pabst, Structures of some tetragonal sheet silicates, Acta Crystallographica 12 (1959) 733-739.

[50] M.J. Buerger, C.T. Prewitt, The crystal structures of wollastonite and pectolite, Proceedings of the National Academy of Sciences, U.S.A. 47 (1961) 1884-1888.

[51] W.H. Baur, In search of the crystal structure of low quartz, Zeitschrift fuer Kristallographie 224 (2009) 580-592.

[52] M. Sato, X-ray study of tridymite, Mineralogical Journal 4 (1964) 115-130.

FIGURE CAPTIONS

Figure 1. Projection of the Kossel cones on the EBSD detector screen, showing the pair of Kikuchi lines and the region included between them (Kikuchi band).

Figure 2. Backscattered electron (BSE) image of a large area of the sample (x50 magnification). Inset: Two of the balls of Egyptian blue found in La Cabañeta (Zaragoza, Spain).

Figure 3. a) Experimental EBSD pattern of cuprorivaite. b) Indexed EBSD pattern of cuprorivaite.

Fig. 4. a) A smaller area of the Egyptian blue pigment showing the presence of cuprorivaite (C, light grey) and glassy phase (Gp, dark grey) (BSE image). b) Image formed with forescattered electrons. c) Phase map (colour codes: blue: cuprorivaite, yellow: quartz, green: tridymite, red: wollastonite). *Band contrast* and *Band slope* components were added to the phase map. Map size: 105x77 pixel (step size 2 μm).

Fig. 5. Phase map of a 2300x1720 μm^2 area (step size 10 μm) (colour codes: blue: cuprorivaite, yellow: quartz, green: tridymite, red: wollastonite). *Band contrast* and *Band slope* components were added to the phase map.

Fig. 6. a) Frequency distribution function of the cuprorivaite grain size obtained from the EBSD map of Fig. 5. b) Frequency distribution function of the cuprorivaite grain aspect ratio obtained from the EBSD map of Fig. 5.

Fig. 7. Stereographic projection of the <100>, <110> and <001> directions of the cuprorivaite grains in the EBSD map of Fig. 5.

TABLE CAPTIONS

Table I. Crystallographic parameters of the studied phases.

Table II. Volume percentage of the different phases obtained by EBSD. The data of the glassy phase and porosity, which correspond to the non-diffracting areas of the maps, were discriminated using image analysis.

Figure 1

Click here to download high resolution image

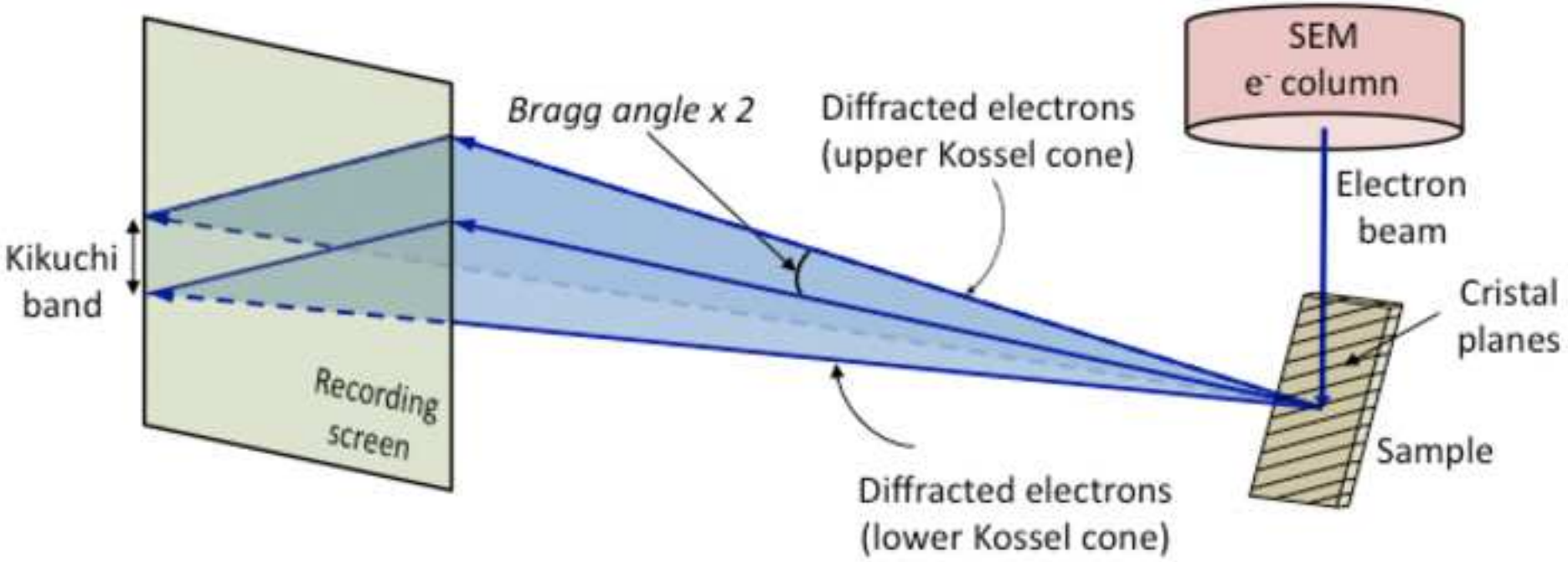

Figure 2

Click here to download high resolution image

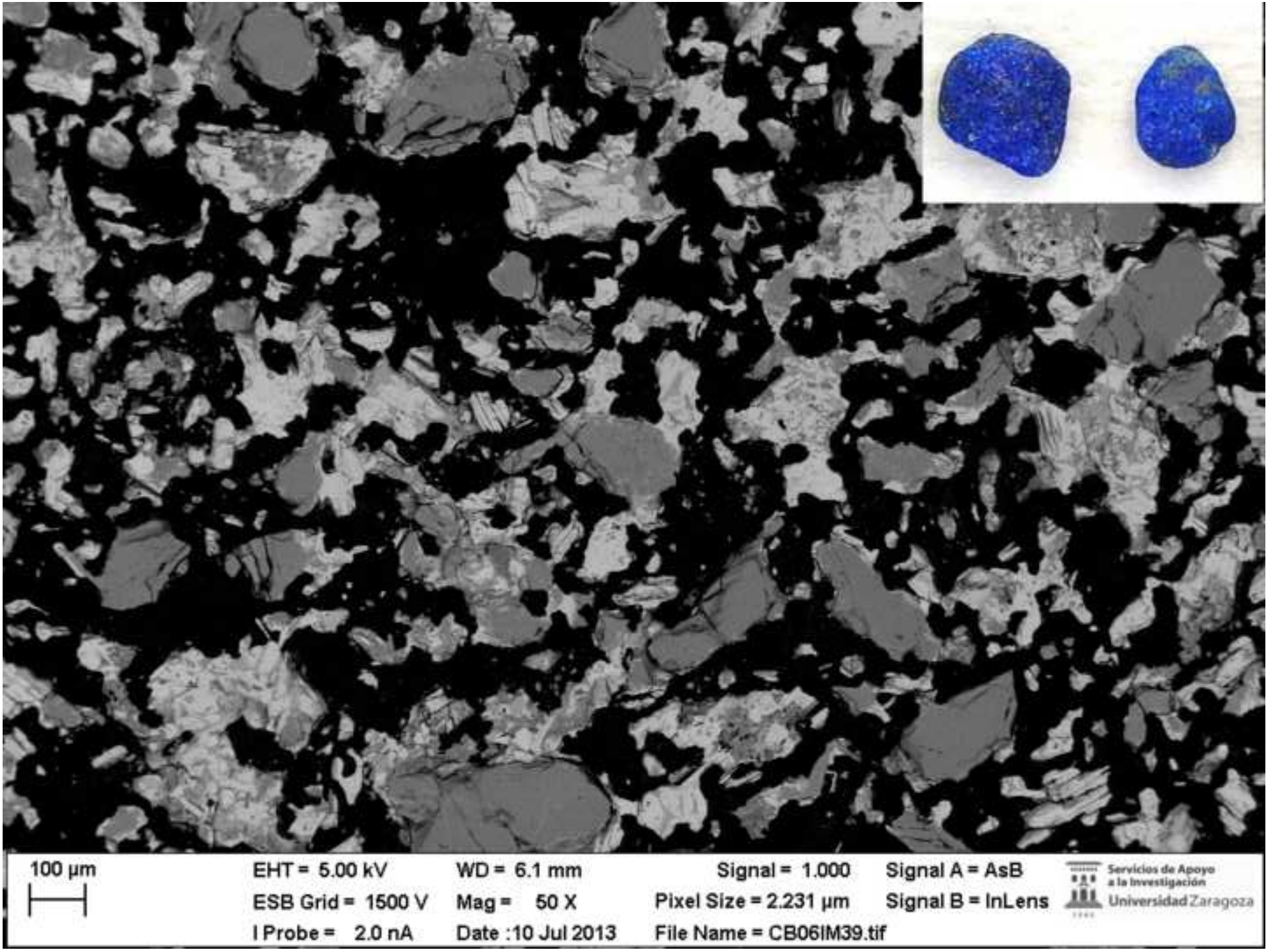

Figure 3a

Click here to download high resolution image

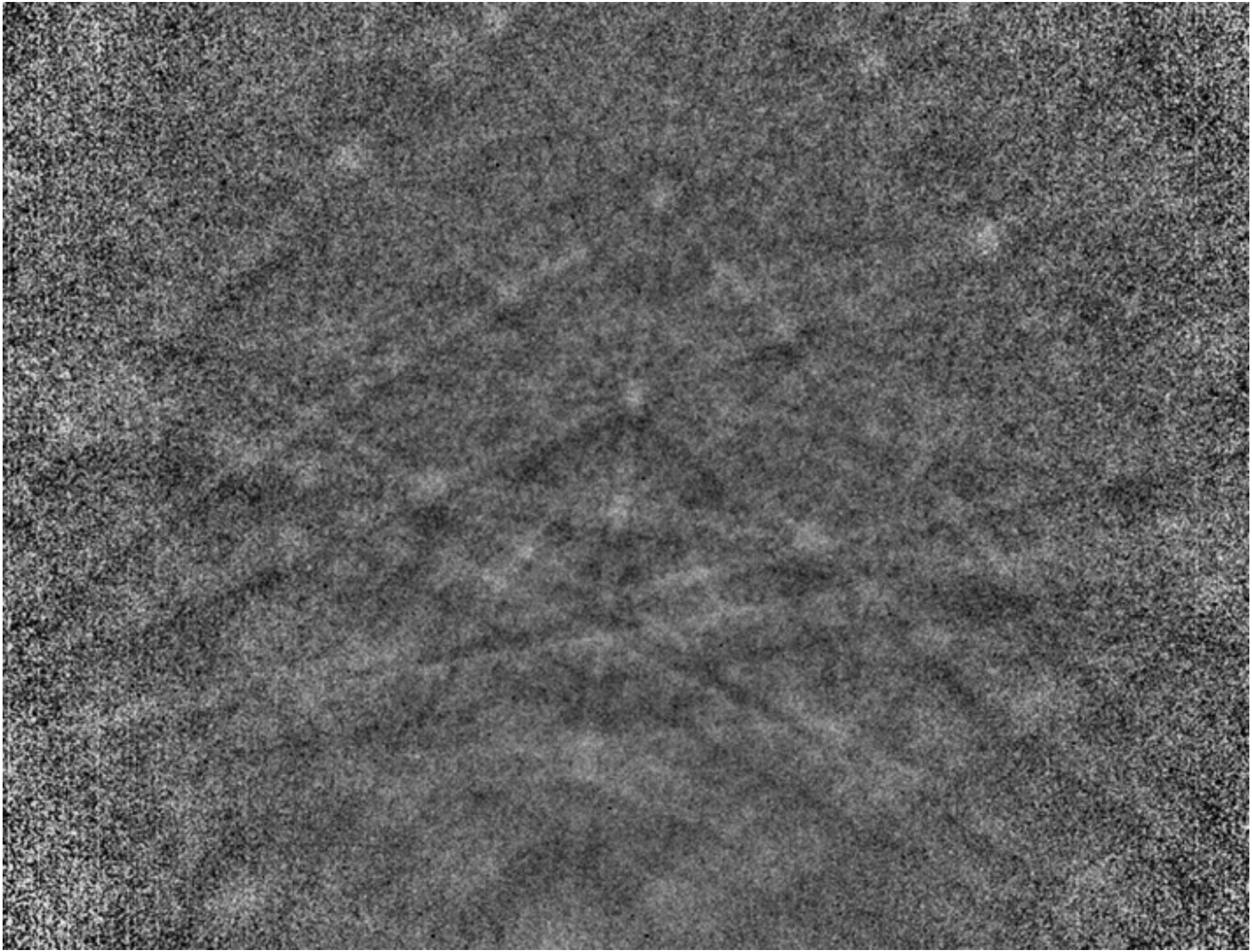

Figure 3b

Click here to download high resolution image

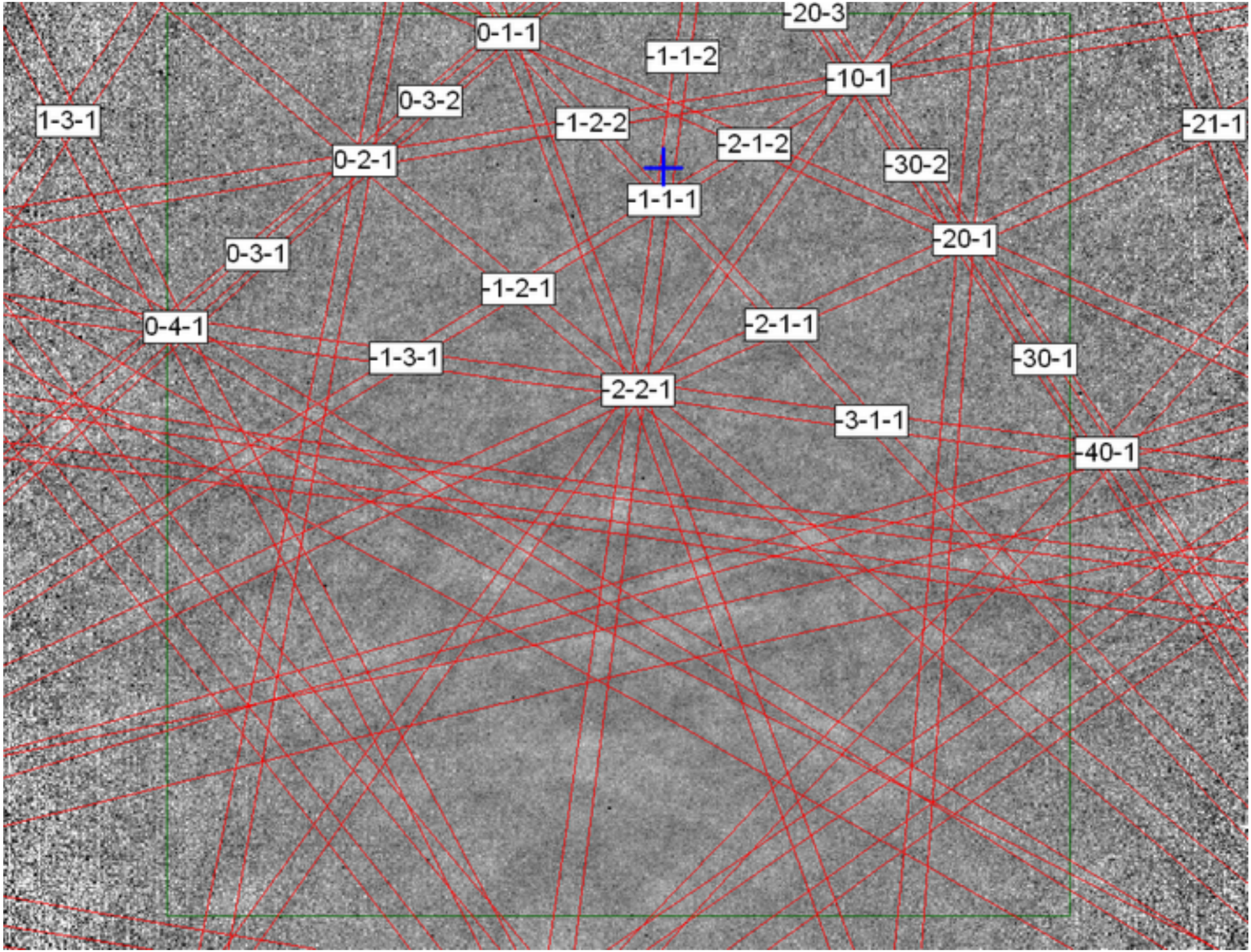

Figure 4a

Click here to download high resolution image

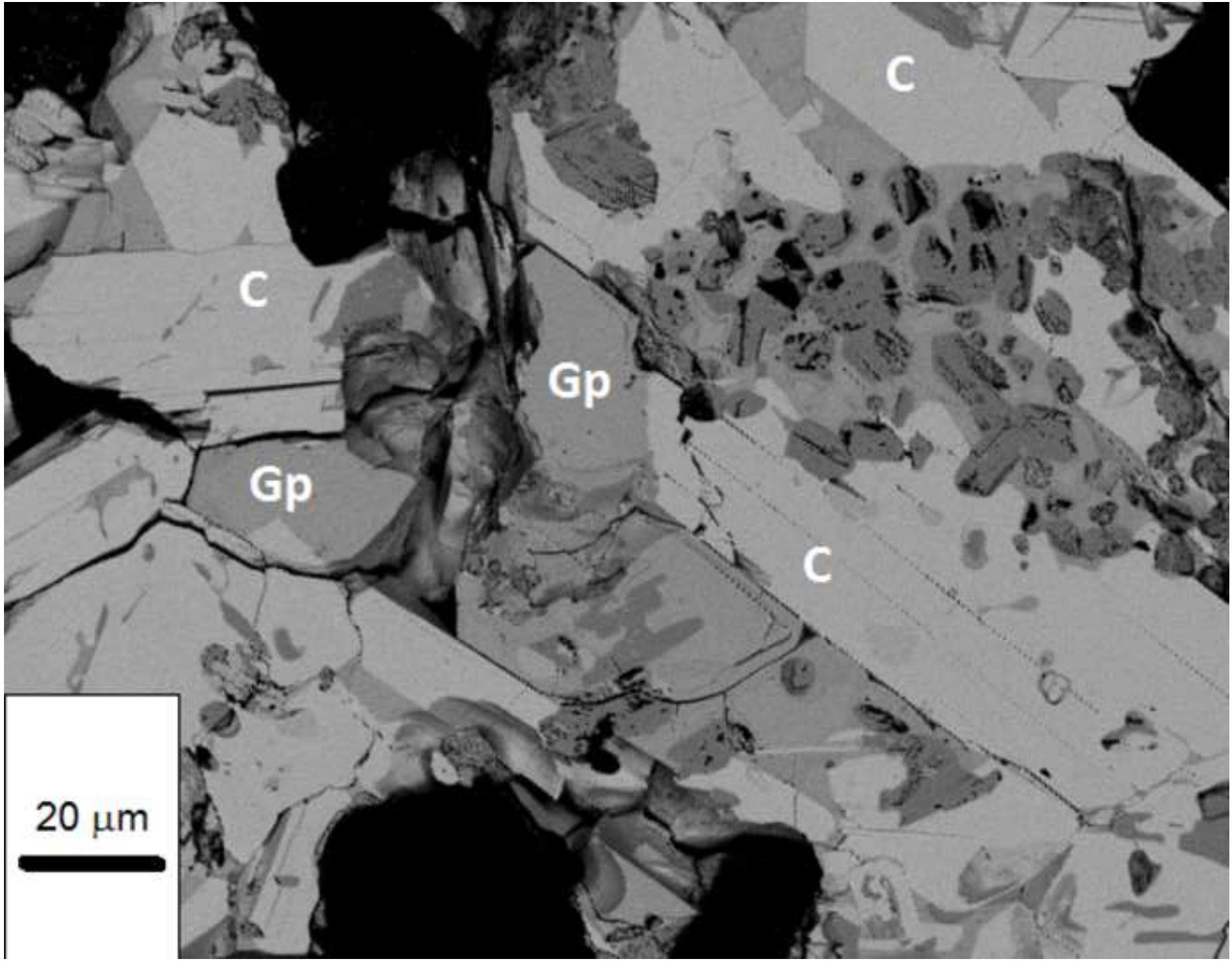

Figure 4b

Click here to download high resolution image

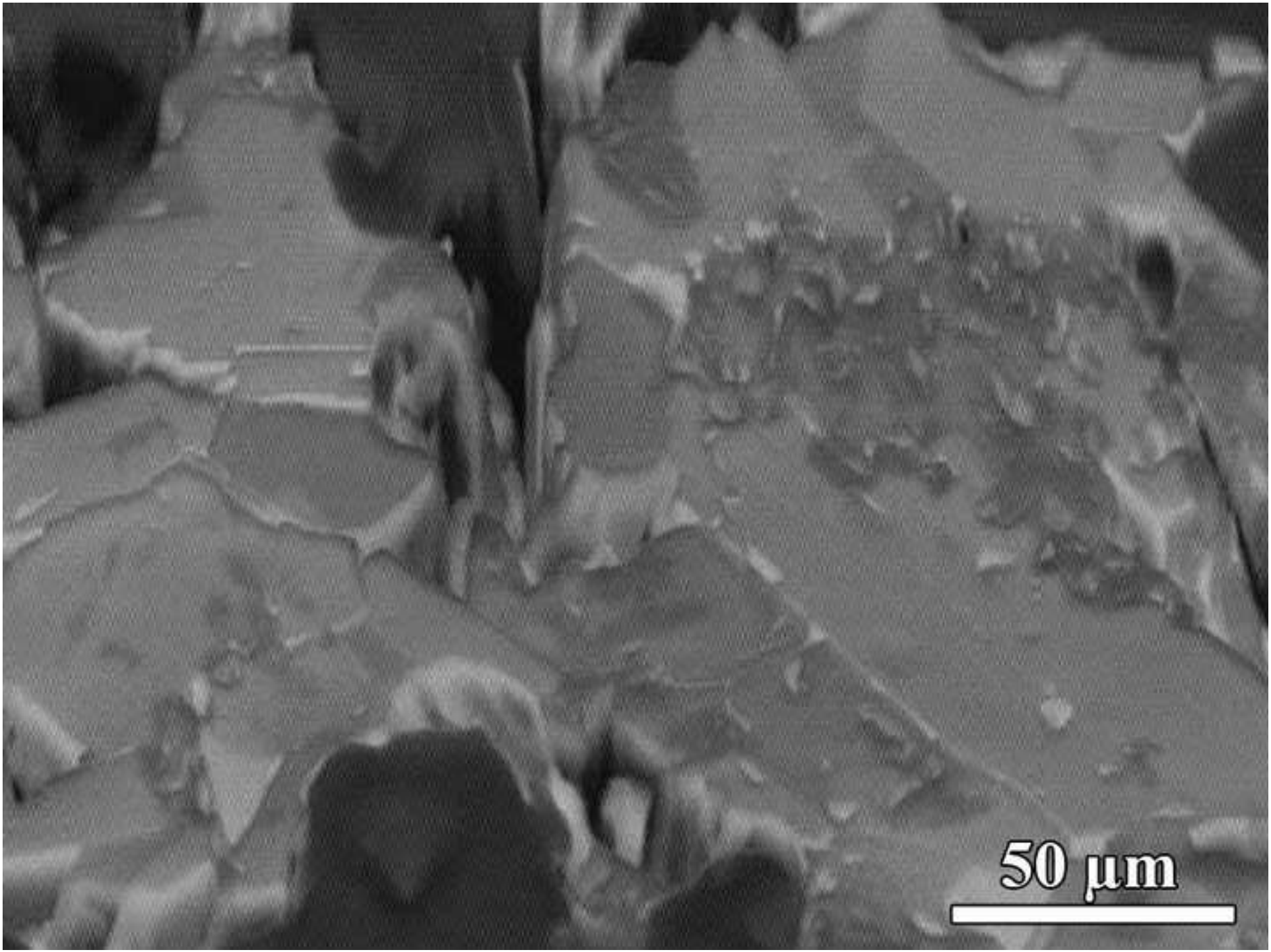

Figure 4c
Click here to download high resolution image

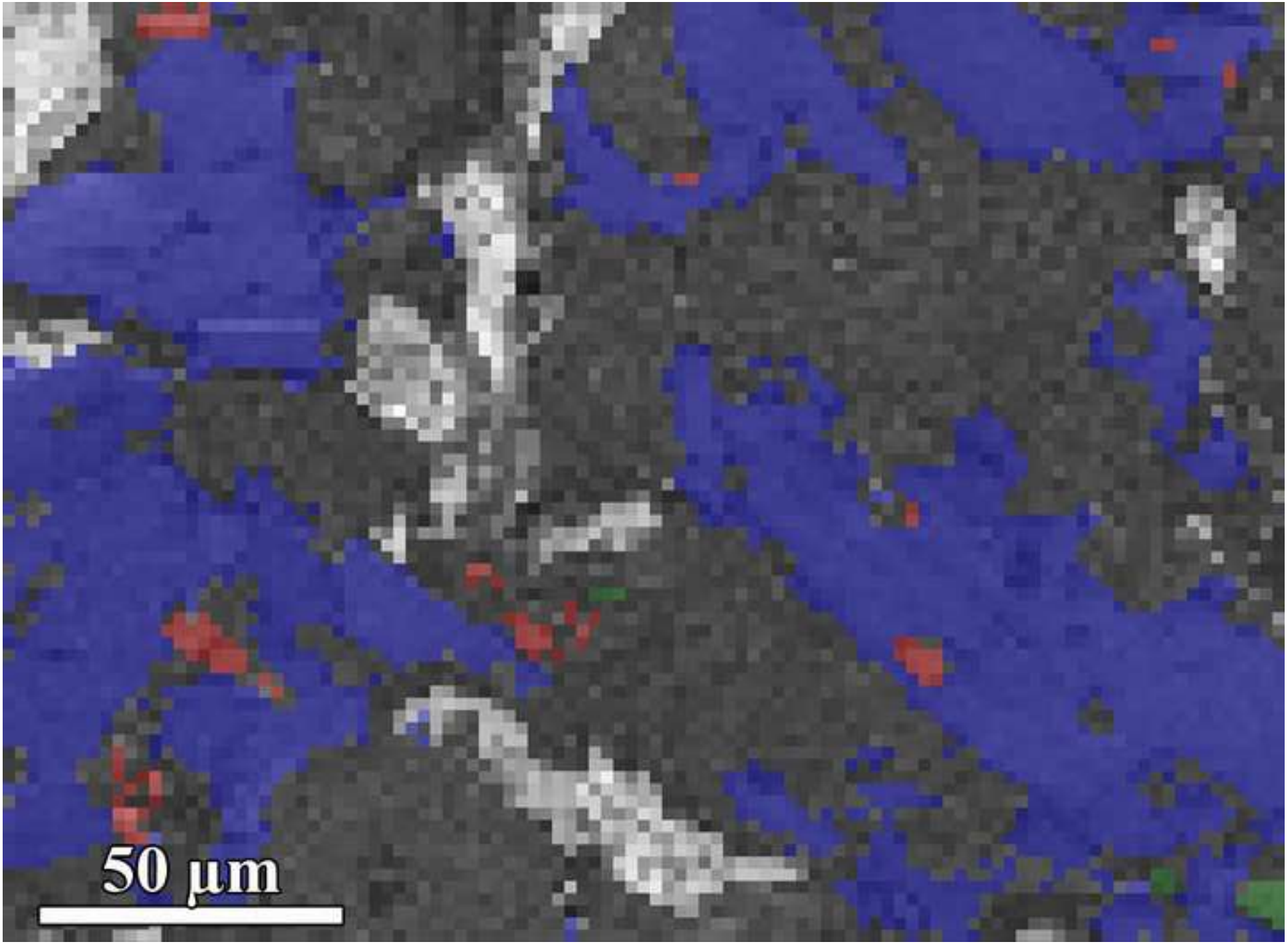

Figure 5

Click here to download high resolution image

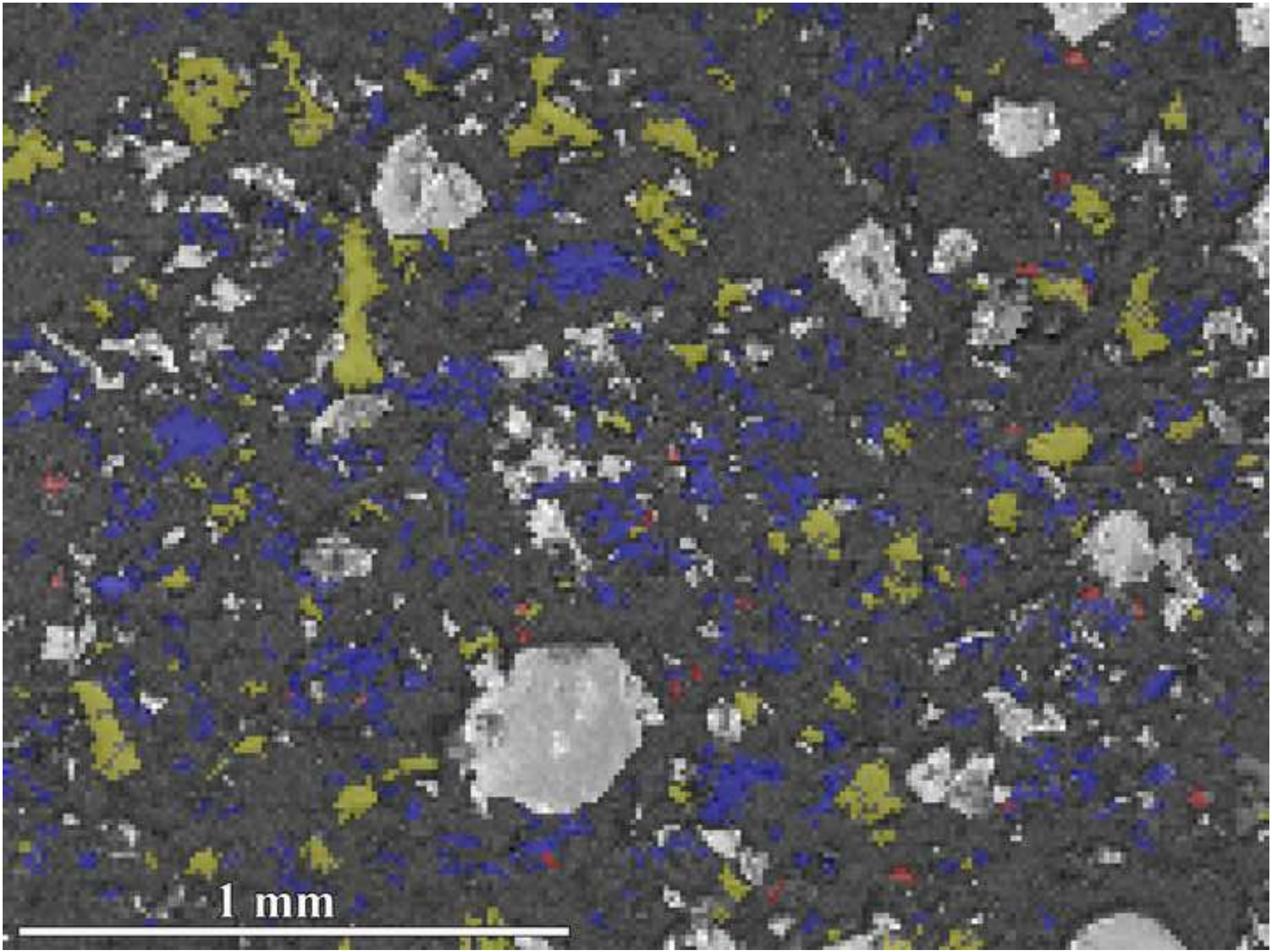

Figure 6a
Click here to download high resolution image

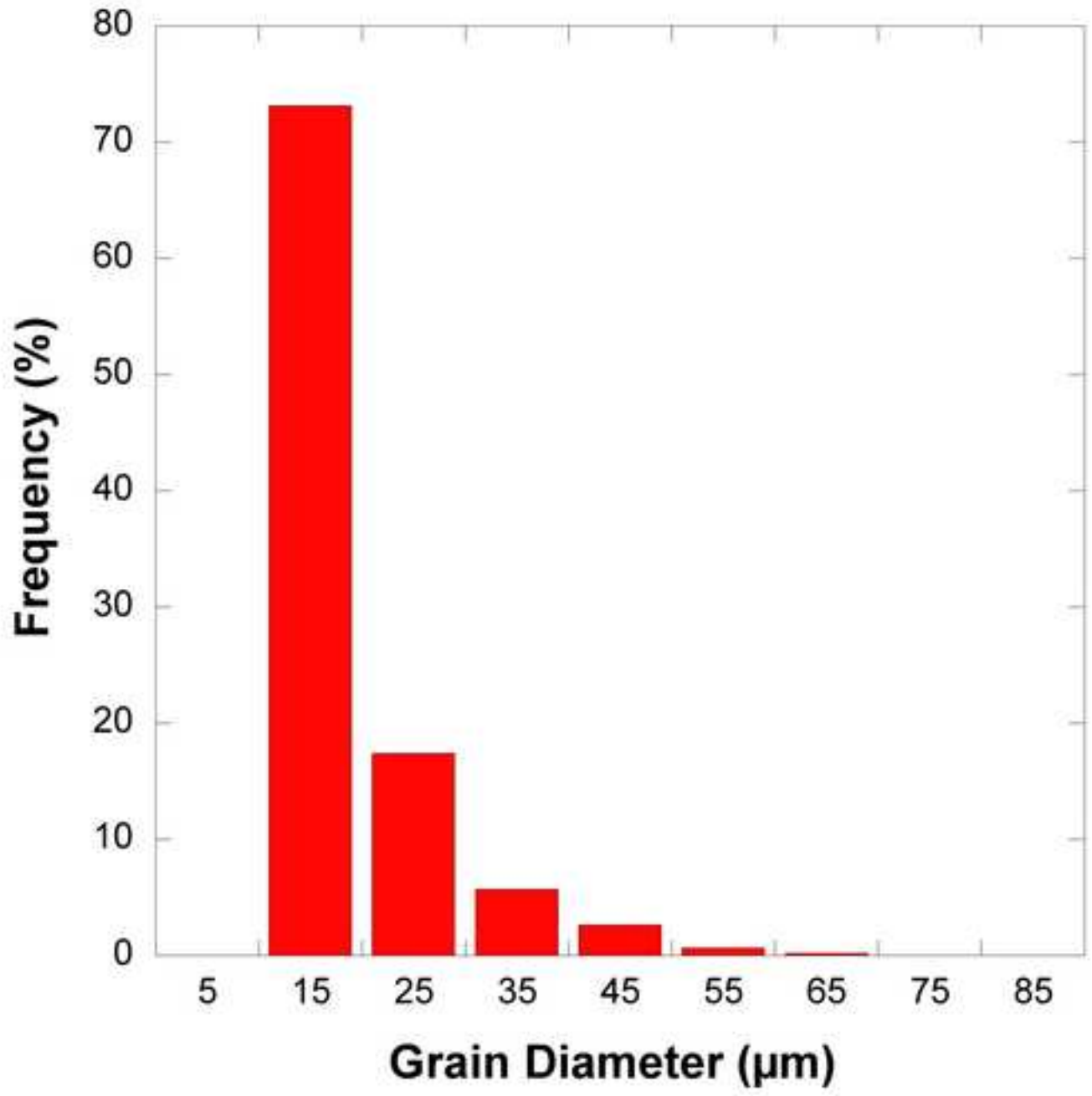

Figure 6b

Click here to download high resolution image

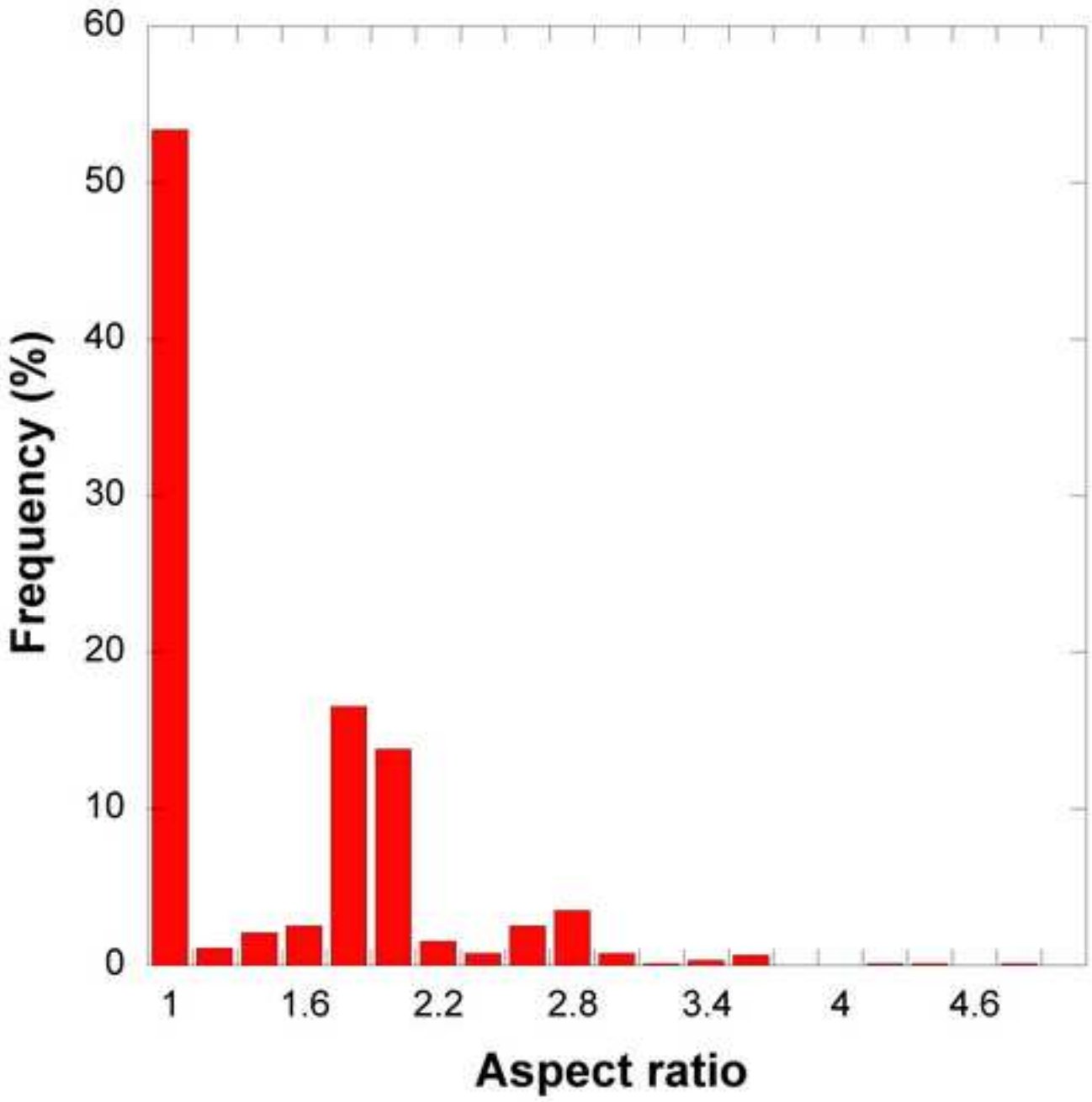

Figure 7

Click here to download high resolution image

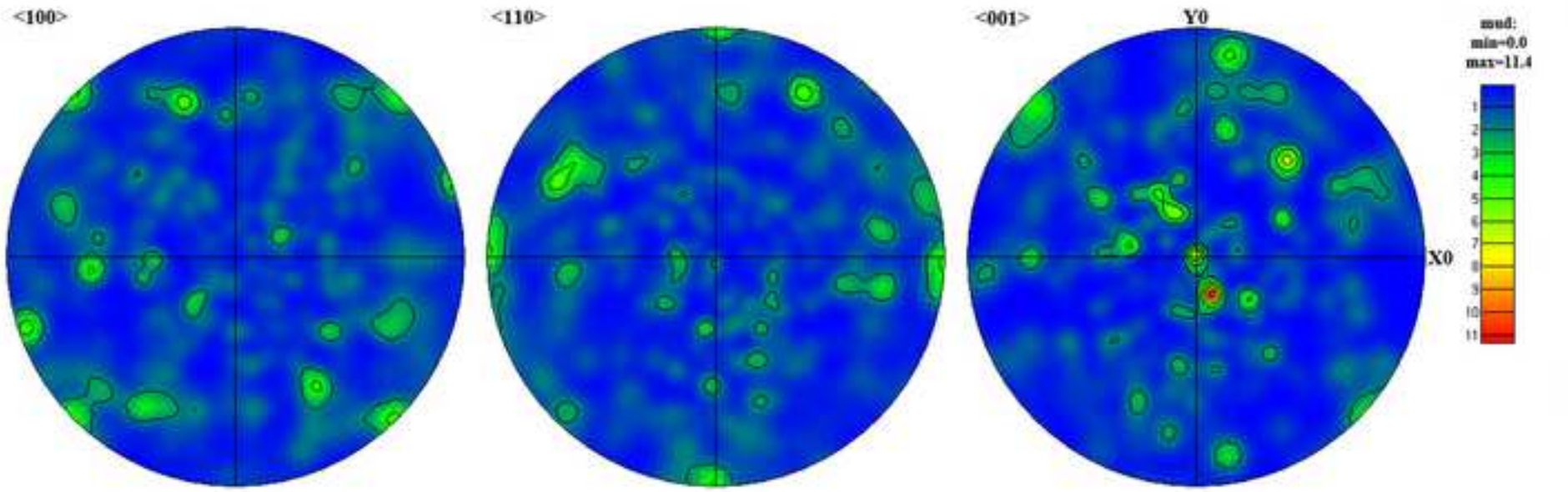

Tables

Table I. Crystallographic parameters of the studied phases.

Name	Composition	Cell (Å, º)	Space Group	Reference
Cuprorivaite	$CaCuSi_4O_{10}$	a=7.301, c=15.12 α=β=γ=90	P4/*nnc*	[49]
Wollastonite	$CaSiO_3$	a=7.94, b=7.32, c=7.07 α=90.03, β=95.37, γ=103.43	P-1	[50]
Quartz	SiO_2	a=4.91, c=5.40 α=β=90, γ=120	$P3_121$	[51]
Tridymite	SiO_2	a=5.03, c=8.22 α=β=90, γ=120	$P6_3/mmc$	[52]

Table II. Volume percentage of the different phases obtained by EBSD. The data of the glassy phase and porosity, which correspond to the non-diffracting areas of the maps, were discriminated using image analysis.

Map Area	Cuprorivaite	Wollastonite	Tridymite	Quartz	Glassy phase	Porosity
388 x 292 μm^2	13.4	0.6	0.4	7.3	34.2	44.1
210 x 154 μm^2	39.1	1.2	0.2	0.0	43.0	16.5
2300 x 1720 μm^2	8.4	0.3	0.0	4.9	39.2	47.2